J. Phys. B: At. Mol. Opt. Phys. 28 (1995) 4593–4606. Printed in the UK

Three-dimensional recoil-ion momentum analyses in 8.7 MeV O^{7+}–He collisions

T Kambara, J Z Tang, Y Awaya, B D DePaola†, O Jagutzki‡, Y Kanai, M Kimura§, T M Kojima, V Mergel‡, Y Nakai, H W Schmidt-Böcking‡ and I Shimamura

The Institute of Physical and Chemical Research (RIKEN), Wako, Saitama, 351–01 Japan

Received 20 July 1995

Abstract. Using high-resolution recoil-ion momentum spectroscopy we have measured the differential cross sections of single-electron capture and target single-ionization processes for 8.7 MeV O^{7+}–He collisions as functions of scattering angle. A transverse momentum resolution of ± 0.2 au, which corresponds to an angular resolution of about $\pm 1.5 \times 10^{-6}$ rad for the projectile scattering angle, was obtained by intersecting a well collimated O^{7+} beam with a target of a supersonic He jet from a pre-cooled gas and by measuring the recoil-ion transverse momentum. For the single capture reaction, information on the n-value of the electron final state in $O^{6+}(1snl)$ is obtained from the longitudinal momentum of the recoil ions. In pure single-electron capture, the dominant contributions to capture were found to be those from the $n = 4$ and higher states, whereas single capture accompanied by the ionization of the second target electron mainly populates $n = 2$ to $n = 4$ states. Furthermore, the measured transverse momentum distribution differs significantly between pure single capture and capture with simultaneous ionization. The measured data for the pure capture process compare favourably with theoretical results based on a molecular-state expansion method. Other experimental data are discussed in terms of the classical overbarrier model.

1. Introduction

The study of inelastic ion–atom collision processes, such as electron capture or ionization, has provided a substantial part of our knowledge on atomic structure and on the dynamics of such collisions. In general the experimental data have provided more information on these processes, as the number of parameters in the differential cross sections have been increased. In this study we have obtained final-state selective angular differential cross sections for pure single-electron capture and for transfer ionization in 8.7 MeV O^{7+} on He collisions by applying a high-resolution recoil-ion momentum spectroscopy, which is a new method of collisional spectroscopy.

Energy-gain spectroscopy has been established as a powerful technique to study the dynamics of charge exchange processes in mainly slow (up to 10 keV/nucleon) highly charged ion–atom collisions (Lorents and Aberth 1965, Ohtani *et al* 1982, Tsurubuchi *et al* 1982, Ohtani 1984, Tawara *et al* 1984, Schmeissner *et al* 1984, Cocke *et al* 1986, Giese *et al* 1986, Barat *et al* 1987, Barat and Roncin 1992). Measuring the change of

† Permanent address: Department of Physics, Kansas State University, Manhattan, KS, USA.
‡ Permanent address: Institut für Kernphysik, Universität Frankfurt, Frankfurt/M, Germany.
§ Permanent address: Argonne National Laboratory, Argonne, IL, USA.

0953-4075/95/214593+14$19.50

kinetic energy of the projectile ions, one can deduce the exchange of internal energy among the collision partners (the Q value) and thus can determine their final electronic states. Depending on the preparation and the energy analysis of the incoming and scattered beam, an energy-gain resolution in the eV regime (Ohtani *et al* 1982, Nielsen *et al* 1985, Giese *et al* 1986, Barat and Roncin 1992) could be achieved in collisions of slow highly charged ions with atoms. This energy-gain resolution corresponds to a relative energy resolution of the projectiles of about 10^{-4}. To identify selected reaction channels the high-resolution energy-gain information was often not sufficient. Therefore, an additional coincidence with emitted recoils, electrons or photons was required (Barat *et al* 1987, Chetioui *et al* 1990). Measuring the energy gain or loss of the projectile as a function of the projectile scattering angle, one can determine differential cross sections for capture into an individual excited state (Barat *et al* 1987).

In comparison to other spectroscopy techniques, e.g. high-resolution electron spectroscopy (Itoh *et al* 1985, Morgenstern *et al* 1990, Mack 1987, Bordenave-Montesquieu *et al* 1987), this energy-gain technique also yielded important information on the impact parameter and thus provided deeper insight into the kinematics of electron-capture processes.

For higher energy ion beams (above 100 keV/nucleon), however, such a resolution was hardly achievable with this traditional energy-gain spectroscopy technique without sophisticated beam preparation devices (Park *et al* 1978, Schuch *et al* 1988, Htwe *et al* 1994). Therefore no differential cross sections for capture into excited states for MeV collisions have been measured so far by this traditional technique.

Recoil-ion momentum spectroscopy (RIMS), another method to measure the Q value and the momentum transfer in a collision, has recently been developed for the study of the collision dynamics. In a collision with a two-body final state without free electrons, the final momentum of the recoil ion provides the same information as the final momentum of the energetic projectile: The longitudinal recoil momentum represents the Q value and the number of transferred electrons whereas the transverse recoil momentum yields complete information on the scattering angle. As shown in section 2 the momentum of a recoil ion is of the order of an atomic unit which corresponds to a velocity of abut 300 m s^{-1} for a He ion. Since the resolution of this method depends on the initial thermal motion in the target atoms, the target is often prepared as a supersonic gas jet.

The method of measuring Q-values by recoil-ion momentum spectroscopy has recently been applied by Ali *et al* (1992), Frohne *et al* (1993), Giese *et al* (1993) and Wu *et al* (1994, 1995). Using a gas-jet target without pre-cooling (warm gas jet), they have measured the recoil-ion longitudinal momentum from various collisions between highly charged ions and atoms. Due to the high gas-jet temperature, their resolution of the recoil momentum was not sufficient to obtain detailed information on the impact-parameter dependence.

Cold target recoil-ion momentum spectroscopy (COLTRIMS) is a newly developed technique (Ullrich *et al* 1994) where the target is prepared as a very cold supersonic gas jet with an internal temperature as low as a few mK and nearly *zero* thermal momentum. One can acquire this low internal temperature by pre-cooling the target gas by a cryogenic system before the formation of the jet. The COLTRIMS technique allows one to measure, with nearly 4π detection efficiency, simultaneously the three-dimensional components of the recoil-ion momentum after the collisions. The momentum transfer can be measured with a high resolution so that the separation of electron capture into different final states becomes possible even in highly energetic collisions. With existing techniques and small devices a recoil-ion momentum resolution better than 0.1 au can be obtained.

In energetic collisions the typical scattering angles of interest are much lower than 10^{-3} rad, where traditional methods to measure the projectile scattering angle can hardly

be applied. However, COLTRIMS provides the momentum resolution required for such measurements even for extremely small projectile scattering angles, i.e. in the 10^{-6} rad regime.

Using COLTRIMS, Mergel *et al* (1995) have recently measured the doubly differential capture cross sections for the symmetrical collision system He^+ on He in the impact-energy regime of 300 to 1000 keV. They were able to distinguish between capture into excited states and capture into the ground state. With increasing projectile energy they observed an increasing contribution of capture into the ground state in agreement with predictions of classical trajectory Monte Carlo (Meng *et al* 1993) and continuum distorted wave (CDW) (Belkić and Gayet 1977) theories.

To study the dynamics of single-electron capture and ionization processes in fast heavy ion–atom collisions, we have used the COLTRIMS method to measure the differential cross sections of capture and ionization in 8.7 MeV O^{7+}+He collisions. Wu *et al* (1994, 1995) have recently studied the longitudinal recoil-ion momentum distribution in O^{7+}+He system using a warm gas-jet target. They separated one-electron capture to the K and higher shells of the projectile and found that the capture to the higher shells dominates at energies below 3.7 MeV u^{-1}. They also studied the longitudinal recoil-ion momentum distribution in transfer ionization process.

In the present work, performing a recoil-projectile coincidence, we have determined the three-dimensional recoil-ion momentum for selected final projectile and recoil charge states and thus measured the Q value distribution with a higher resolution and obtained differential cross sections of the single-electron capture and the transfer ionization processes.

To account theoretically for the dynamical features of the pure capture process and to identify the dominant channels of the charge transfer, we have performed a semiclassical close-coupling calculation based on molecular representation of the electronic states. The differential cross sections have been calculated as functions of the recoil-ion transverse momentum and have been compared with the experimental results. The measured data have also been compared with the classical overbarrier model (Ryufuku *et al* 1980).

2. Recoil-ion kinematics

In this section we briefly present the kinematical characteristics of the recoil-ion momentum by a collision, which are derived from total energy and momentum conservation in a non-relativistic framework. All the quantities hereafter are expressed in the laboratory frame in which the target atom is at rest before the collision. The transverse and longitudinal components of the recoil-ion momentum can be separately approximated by simple formulae if the following three conditions are well fulfilled: (i) the change in the binding energy of the electrons is much smaller than the projectile kinetic energy; (ii) the projectile is much heavier than the electron; and (iii) the projectile scattering angle is much smaller than 1 rad. These conditions are generally valid for fast (but non-relativistic) ion–atom collisions like the one considered here.

For example in a case where single-electron capture is accompanied by single target-electron ionization, the longitudinal (parallel to the projectile velocity) component of momentum $p_{\parallel R}$ is

$$p_{\parallel R} = (E_e - Q(n))/v_P - m_e v_P/2 - p_{\parallel e} \tag{1}$$

and the transverse (perpendicular to the projectile velocity) component $p_{\perp R}$ is

$$p_{\perp R} = -p_{\perp P} - p_{\perp e} \tag{2}$$

where $Q(n)$ is the difference between the initial and final electronic binding energies when the electron is captured into the projectile n-shell, E_e is the final kinetic energy of the ejected electron, v_P is the projectile velocity, and $p_{\parallel e}$, $p_{\perp e}$, and $p_{\perp P}$ are the electron and projectile final momentum components. It is easy to see that the recoil-ion longitudinal momentum for the case of pure capture (i.e. no electron in the continuum) has two contributions. The first term is due to the electronic binding energy, which changes the nuclear kinetic energies in the centre-of-mass system. For example, the recoil ion gains kinetic energy and thus an additional backward momentum of 5.6 au when an O^{7+} ion captures an electron to its 1s orbit. The second term results from the electron mass-transfer from the target to the projectile inertial frame and is independent of the final excited state in the projectile. This term yields a backward momentum of 2.34 au for the system investigated here ($v_P = 4.68$ au). For a pure capture process the recoil-ion longitudinal momentum thus has a definite value corresponding to each combination of the projectile and target electronic states. Since the COLTRIMS system used here provides a resolution of about ± 0.5 au or better for the recoil-ion longitudinal momentum, capture into the 1s or higher n states can be separated experimentally.

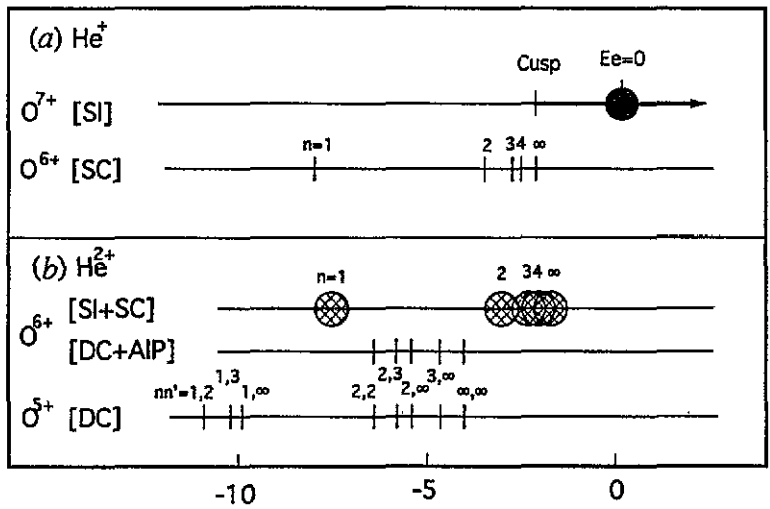

Figure 1. Recoil-ion longitudinal momentum $p_{\parallel R}$ for 8.7 MeV O^{7+}+He collisions calculated with (1): (*a*) displays the momenta for recoil He^+ ions from the pure single ionization (SI) with outgoing O^{7+} and pure single capture (SC) with O^{6+}, and (*b*) displays those for recoil He^{2+} from transfer ionization with outgoing O^{6+} and double capture (DC) with O^{5+}. The hatched circles show the expected momentum broadening due to the momentum of the ejected free electron. See the text for details.

To demonstrate the capability of COLTRIMS to resolve the processes leading to different final states, we present the longitudinal momentum components ($p_{\parallel R}$) in our collision system (O^{7+}+He) in figure 1: figure 1(*a*) is for He^+ recoil ions and (*b*) for He^{2+} ions when they are detected in coincidence with the different final projectile charge states.

The upper line in figure 1 shows the $p_{\parallel R}$ for pure single-electron ionization (SI). The bold part of the line shows the range of $p_{\parallel R}$ which is kinematically allowed. According to (1) the backward momentum of the recoil ion (negative $p_{\parallel R}$) has a maximum when the electron is emitted with the same velocity as the projectile (*cusp*). If the *cusp* is a considerable part of the total electron emission cross section, a peak should be observable at $p_{\parallel R} = -2.1$ au in the recoil-ion momentum spectrum. On the other hand, most of the recoil ions distribute

around $p_{\parallel R} = 0$ with a width which corresponds to the momentum spread of an electron in a He atom, since the SI process is mainly due to distant collisions with little momentum exchange between the projectile and the target. This spread is schematically indicated in the figure by a hatched circle with a diameter of 1 au. If the momentum distribution of the emitted electron is symmetric in the forward and backward directions, the distribution might be centred at about $p_{\parallel R} = 0.2$ au (in the forward direction) due to the negative Q-value and the final electron kinetic energies.

Only pure single-electron capture (SC) can contribute to the He^+/O^{6+} reaction channel. On the second line in figure 1(*a*), the values of $p_{\parallel R}$ for different principal quantum numbers n of the final $O^{6+}(1snl)$ are shown. The $p_{\parallel R}$ from SC to the $n = \infty$ state is equivalent to that from *cusp*. Even with a resolution of only ± 0.5 au, one sees that the capture to the ground state and the $n = 2$ states can be separated from the capture into the higher states.

The transfer-ionization (TI) channel yielding O^{6+} and He^{2+} with one free electron in the final state is fed by two processes: (i) single-electron capture accompanied by direct single target electron ionization (SI + SC); and (ii) double-electron capture into higher projectile states followed by autoionization of the projectile (DC+AIP). These processes can be distinguished by their different recoil momenta $p_{\parallel R}$ which are shown on the upper two lines in figure 1(*b*). The $p_{\parallel R}$ distribution from the SI + SC process is centred at discrete values corresponding to the different states of $O^{6+}(1snl)$ as in the case of SC. Since another electron is ejected from the target in SI + SC, the $p_{\parallel R}$ is larger by about 0.4 au than that from SC due to the smaller Q value and has additional broadening due to the kickback of the ejected electrons. To first order this broadening is expected to be identical to that from pure single ionization (SI). The broadening is indicated in figure 1(*b*) by hatched circles with the same diameter as in the SI process.

In the case of double electron capture, the second term in (1) should be multiplied by a factor of two due to the two-electron mass transfer from the target to the projectile. The recoil-ion momentum $p_{\parallel R}$ takes discrete values corresponding to the binding energies of $O^{5+}(1snln'l')$. Since the recoil-ion momentum is not affected by a subsequent autoionization of the projectile, the values of $p_{\parallel R}$ from DC + AIP are identical to those from pure double electron capture (DC) without subsequent autoionization but the states with $n = 1$ or $n' = 1$ cannot contribute to the DC + AIP. The reaction channel He^{2+}/O^{5+} contains only the DC process. The values of $p_{\parallel R}$ are shown in figure 1(*b*) for the pure DC and DC + AIP.

The recoil transverse momentum in (2) has a contribution from the scattering of projectile and the kickback of the ejected electrons. In the case of pure capture without free electrons, the recoil and the projectile transverse momenta yield, therefore, identical information on the ion–atom trajectories.

3. Experimental set-up

The experiment was performed at the heavy-ion linear accelerator (RILAC) at RIKEN. An O^{3+} beam of 8.7 MeV from the accelerator was post-stripped by a carbon foil and charge-state analysed by a bending magnet. The resulting O^{7+} beam of 8.7 MeV was collimated by two sets of adjustable collimators with apertures of 0.6×0.6 mm^2 and 4 m apart from each other, thus yielding a beam size less than 1 mm at a target position. The projectiles had a velocity of 4.68 au and a momentum of 1.37×10^5 au. Although a considerable fraction of the O^{7+} ions can be excited in the stripper into the $2s_{1/2}$ metastable state, only a small fraction (about 2×10^{-3}) of them would survive on their way (20 m) to the target since the ion flight time is about four times the lifetime of the metastable state and the metastable ions are quenched in the field (about 0.16 T) of the bending magnet (Leventhal *et al* 1972,

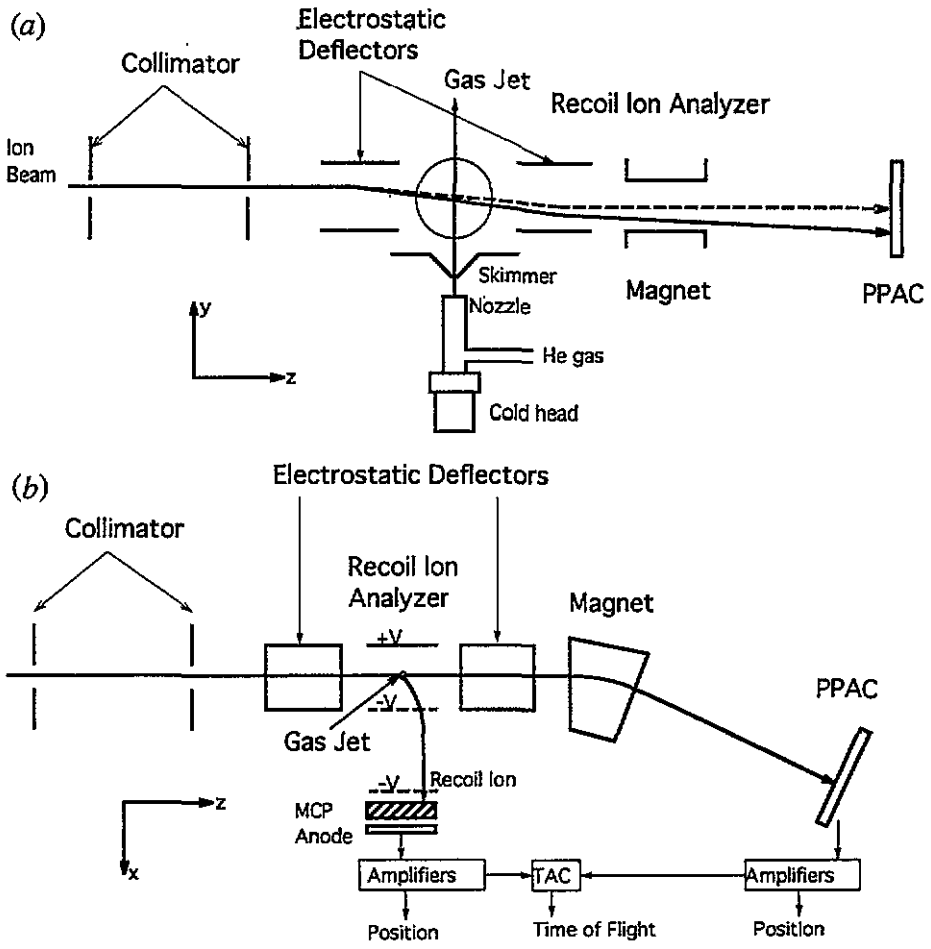

Figure 2. Schematic diagram of the experimental set-up: (*a*) shows the vertical cross section of the apparatus and (*b*) shows the horizontal cross section and the circuit system. The broken line in (*a*) indicates the trajectory of contaminant ions which have captured an electron before the first deflector and the full line that of the ions which have captured an electron between the two deflectors. Cartesian coordinates to define the momentum components are also shown in each of the figures.

Lawrence *et al* 1972).

In figure 2 a schematic diagram of the experimental set-up is presented. We define Cartesian coordinates with the z axis in parallel with the beam direction and the y axis in the jet direction.

The collimated beam intersected a very cold supersonic He jet at the centre of a vacuum chamber with a diameter of 50 cm. The He gas which was pre-cooled by a cryogenic system to approximately 35–40 K at a gas pressure of 220 mbar was expanded upward through a nozzle of about 30 μm diameter into the lower part of the vacuum chamber (first stage) forming a supersonic gas jet (Brusdeylins *et al* 1989, Mergel 1994, Mergel *et al* 1995). The pressure in this first stage was about 5×10^{-4} mbar. The inner part of this supersonic jet passed through a skimmer of 0.5 mm diameter into the upper part of the chamber (main reaction chamber). The distance from the nozzle to the skimmer was about 6 mm. The

internal temperature of the passing supersonic jet was estimated to be about 250 mK. The diameter of the jet at the intersection point was about 2.5 mm. The supersonic jet was finally collected by an evacuated dump on the opposite side of the reaction chamber. The rest-gas pressure in the reaction chamber was about 10^{-7} mbar.

The projectiles were charge state analysed downstream of the chamber by a 25° deflecting magnet and detected with a position-sensitive parallel-plate avalanche detector (PPAD). The projectile O^{7+} beam was contaminated by ions with different charge states through charge-exchange collisions with residual gas in the beam line prior to entering the target region. We set two pairs of parallel plate electrodes; one before and the other after the target. In the measurements of electron capture by the projectiles, the beam was vertically deflected by an electrostatic field before the target and deflected back after the target so that the ions which changed the charge state in the target took a different trajectory from the contaminant ions and they were separated at the PPAD.

The slow recoil ions produced in the intersection region were analysed by a recoil-ion momentum spectrometer (Mergel *et al* 1995) where the ions were extracted by a weak, uniform electrostatic field, passed through a field-free region and hit a position-sensitive detector. By measuring the recoil-ion position and its time-of-flight (TOF) by a coincidence with the detected projectile, the complete recoil-ion momentum vector p_R can be determined. The extraction field was set between 0.67 and 1.33 V cm^{-1} in most of the measurements although it was set to 33 V cm^{-1} to measure the position and size of the intersection region. The momentum resolution was determined by the internal target temperature, the angular divergence of the jet flow and the size of the intersection region between the jet and the beam. The momentum spread due to the internal temperature and the divergence was estimated to be about ±0.1 au. Since the size of the intersection region is about 2.5 mm in the longitudinal and less than 1 mm in the transverse direction, the resolution of the transverse momentum components (±0.16 au) is better than the longitudinal one (±0.4 au). Therefore the resolution of the longitudinal momentum component was estimated to be about ±0.5 au, and that of the transverse component to be about ±0.2 au. The zero position in momentum space was determined from the recoil-ion distribution for the pure ionization channel and the off-set of the supersonic gas jet with respect to the recoil-ion position resulting from rest-gas ionization. The zero position in the longitudinal momentum is uncertain by about ±0.25 au.

The two-dimensional position information from both detectors was obtained by using a 'wedge and strip' anode structure, where the three charge signals for each particle detection were recorded in list mode by using standard electronic devices.

The experiment yields all momenta simultaneously thus providing reliable results of the relative differential cross sections. To obtain absolute cross sections the absolute target thickness and the overlap integral of supersonic jet and ion beam has to be known. Since this overlap integral was not measured in the present experiment, the measured momentum distribution was integrated over the momentum and normalized to the total cross sections in the literature: The sum of the cross sections of the single electron capture (SC) and the transfer ionization (TI) was determined to be 2.64×10^{-17} cm^2 from an extrapolation of the projectile charge-change cross section from O^{7+} to O^{6+} measured by Dillingham *et al* (1981) and each cross section was determined from the TI to SC ratio measured by Shinpaugh *et al* (1992). The SC cross section was thus estimated as 9.2×10^{-18} cm^2 and the TI cross section to be 1.72×10^{-17} cm^2.

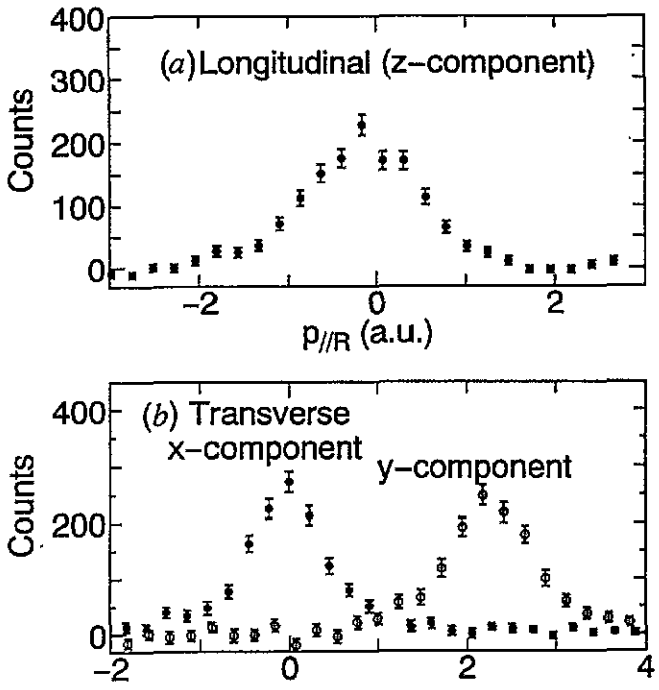

Figure 3. Measured recoil-ion momentum distribution for the pure single ionization (SI) process: (*a*) displays the longitudinal recoil-ion momentum $p_{\parallel R}$ distribution (*z*-axis in figure 2); and (*b*) the transverse momentum $p_{\perp R}$ distributions where full circles show the momentum component perpendicular to the jet (*x*-axis) and open circles in the direction of the jet (*y*-axis). The error bars indicate the statistical uncertainties only. The off-set from zero of the *y*-component is due to the upward motion of the He atoms in the jet with about 2 au momentum.

4. Results and discussion

4.1. Results

In figure 3 the measured recoil-ion momentum distributions are presented for the single ionization reaction (SI):

$$O^{7+} + He \rightarrow O^{7+} + He^{+} + e^{-} \tag{3}$$

as functions of the components of the recoil-ion momentum. The abscissa in figure 3(*a*) is the longitudinal (*z*-direction) component, $p_{\parallel R}$, of the recoil ions and that of figure 3(*b*) is their transverse (*x*- and *y*-directions) component, $p_{\perp R}$ (see figure 2 for definition of the coordinate system). The centroid of the recoil momentum distribution in the *y*-direction is shifted by about 2 au, which results from the initial motion of the He atoms in the jet flow with a velocity of about 600 m s^{-1}. Recoil ions are ejected in the forward as well as in the backward direction. No structure is observed at $p_{\parallel R} = -2.1$ au where the *cusp* electrons are expected (see section 2 and figure 1). The present statistics for this reaction channel does not allow any conclusion on the *cusp* formation in these collisions.

For the pure single-electron capture (SC)

$$O^{7+} + He \rightarrow O^{6+} + He^{+} \tag{4}$$

the longitudinal momentum $p_{\parallel R}$ distribution is displayed in figure 4(*a*) and the differential cross sections $d\sigma/dp_{\perp R}$ are displayed in (*b*) as functions of the transverse momentum

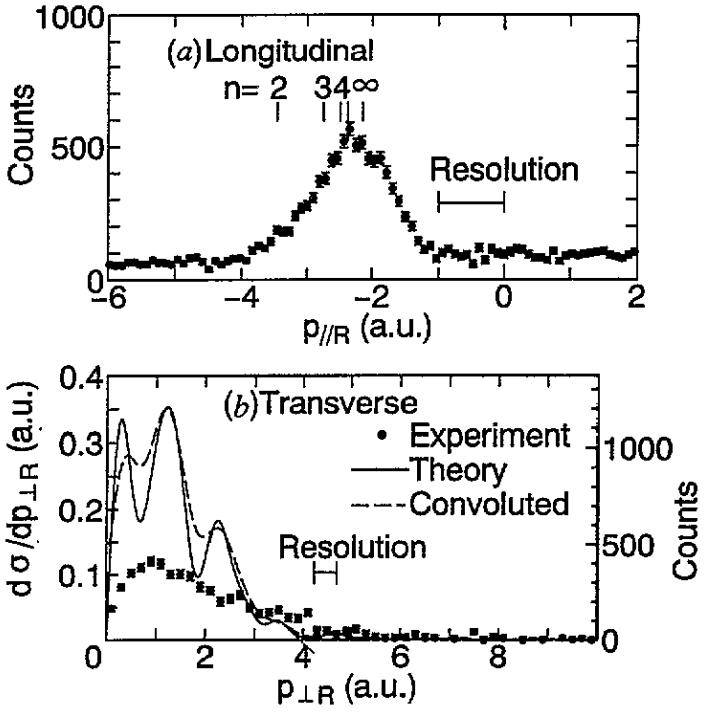

Figure 4. Measured recoil-ion momentum distribution for the pure single-capture reaction channel (SC): (*a*) displays the longitudinal momentum $p_{\parallel R}$ distribution and (*b*) the differential cross section as a function of the transverse momentum $p_{\perp R}$. The *n*-values in (*a*) correspond to the final principal quantum number in $O^{6+}(1snl)$ calculated from (1). The full curve in (*b*) shows the results of the close-coupling calculations and the broken curve shows the results convoluted by the experimental resolution.

component $p_{\perp R}$ of the recoil ion. As expected from (1) all capture processes produce backward ejected recoil ions (see figure 4(*a*)). The plotted *n*-values indicate where, for different final capture states, the recoil-ion momenta are expected due to energy gain in the capture process. From the figure, we can see that the capture predominantly occurs into the $n > 3$ states and capture into the $n = 2$ or $n = 1$ is very weak. The resolution is, however, not sufficient to resolve the higher *n* states. Transforming the measured recoil-ion momentum resolution into the corresponding resolution of a projectile energy-gain measurement, we obtain about $\pm 7.5 \times 10^{-6}$. It is interesting to note that this very good energy-gain resolution was attained with a projectile beam whose initial relative momentum width was in the 10^{-4} range. The recoil-ion momentum resolution is, to first order, not affected by the 'quality' of the incoming beam in contrast to the case of a projectile energy-gain spectroscopy where a resolution of the energy gain is the same order of magnitude as the projectile momentum width. Figure 4(*b*) shows the corresponding transverse momentum distribution (integrated over the whole peak structure in figure 4(*a*)) along with the results of semiclassical close-coupling calculations which are described later.

The $p_{\parallel R}$ distribution is shown in figure 5(*a*) and $d\sigma/dp_{\perp R}$ in figure 5(*b*) for the transfer-ionization process which is a capture of one electron and simultaneous ionization of the other He electron:

$$O^{7+} + He \rightarrow O^{6+} + He^{2+} + e^{-}. \tag{5}$$

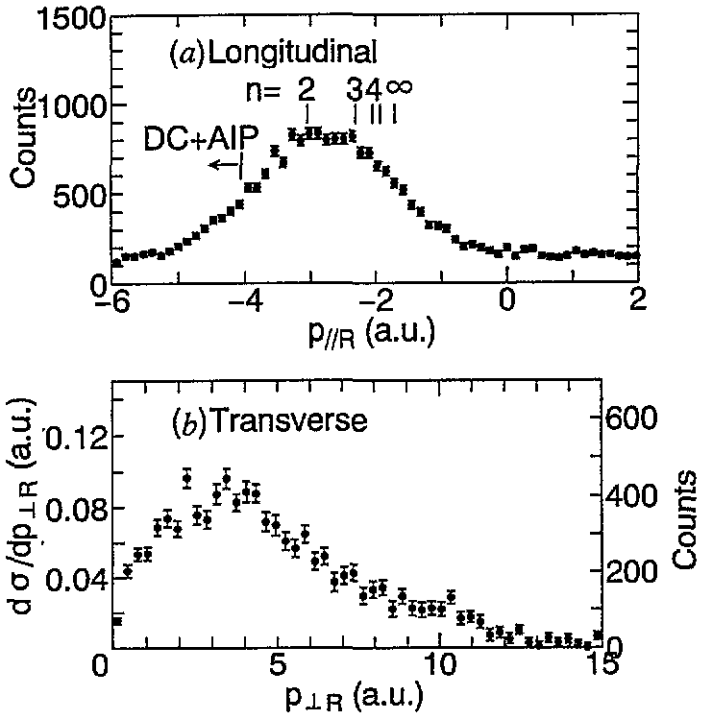

Figure 5. Measured recoil-ion momentum distributions for the transfer-ionization (TI) channel with final O^{6+} and He^{2+} ions: (*a*) displays the longitudinal momentum $p_{\parallel R}$ distribution and (*b*) the differential cross section as a function of the transverse momentum $p_{\perp R}$. Also shown in (*a*) are the principal quantum numbers n of the final electronic states of $O^{6+}(1snl)$ where a single electron capture preceded by a single ionization (SI + SC) is assumed and the highest possible longitudinal recoil momentum in a double capture followed by a projectile autoionization (DC + AIP).

Here the longitudinal momentum $p_{\parallel R}$ is distributed above -5 au and the distribution is broader than for the pure electron capture reaction (see figure 4). Comparing with figure 1, we conclude that the transfer ionization is mainly through single-electron capture (into $n = 2$ and 3 with the highest probability) accompanied by a single target ionization (SI + SC). The contribution of another possible process, double-electron capture followed by autoionization of the projectile (DC + AIP), is relatively small.

4.2. Comparison with classical overbarrier model

Some of the features of the electron-capture processes were examined based on the simple classical overbarrier (COB) charge-exchange model (Ryufuku *et al* 1980), although this model is usually applied to much slower collisions. The COB model defines a critical internuclear distance R where the electrostatic barrier between the colliding ions is so reduced that a He electron in the 1s orbital can pass the barrier into a projectile excited orbital. For SC from a neutral He atom to O^{7+}, the critical internuclear distance R is approximately 8–10 au and the principal quantum number n of the state of the captured electron is about 4 to 5 which is in agreement with the experimental observations shown in figure 4. If a pure Coulomb scattering is assumed on the outgoing part of the trajectory (after the capture process) between O^{6+} and He^{+} which are regarded as point charges,

the recoil-ion transverse momentum is about 0.2 au. This is in rough agreement with the experimental observation in figure 4, where the SC contributions result from collisions with larger transverse momenta than 0.2 au.

For the transfer-ionization channel (5), it is found that the electron is captured into lower states compared to the SC. This is also predicted by the COB model, if the transfer ionization is described as independent ionization and capture in which the ionization precedes the capture process (SI + SC). In this case the O^{7+} ion first ionizes a He atom (3) and then captures the remaining electron from the He^+ ion:

$$O^{7+} + He^+ \rightarrow O^{6+} + He^{2+}. \tag{6}$$

Since the recoil-ion momentum is only weakly affected by the SI process, the final recoil-ion momentum distribution for this transfer-ionization channel provides information on the differential cross sections for electron transfer between ions. To our knowledge, such differential capture cross sections for ion–ion collisions like (6) have never been measured. Since the binding energy of the electron in He^+ is larger than that in a neutral He atom, this process is enabled at a smaller internuclear distance and a lower potential barrier between the ions than in the SC for a neutral He target (4). From the COB model for an unscreened He nucleus, we have an n-value of about 3 and a critical internuclear distance R of about 4.5 au. The transverse recoil momentum from the SI + SC is predicted by COB to be larger than that from the SC since the Coulomb scattering is larger by a reduced screening of the He nuclear charge and by smaller internuclear distances. We obtain the recoil-ion transverse momentum $p_{\perp R} = 0.8$ au for the critical internuclear distance of 4.5 au. This is also in rough agreement with the experimental observation in figure 5, where most of the cross section is from collisions with larger transverse momenta than 0.8 au.

In spite of these agreements, a further comparison of the differential cross sections with the COB seems meaningless since the electron capture cross section predicted by the COB, $\sigma_{COB} = \pi R^2/2$, is larger by two orders of magnitude than the experimental total cross section for single-electron transfer.

4.3. Semiclassical close-coupling calculations

Figure 4(*b*) includes the results of transverse-momentum-dependent cross section $d\sigma/dp_{\perp R}$ from semiclassical close-coupling calculations. Since the details of the theoretical method are described by Kimura and Lane (1989), only a brief description is presented here.

First, we assume a classical, constant-velocity rectilinear motion of the projectile. The electronic motion is described by a wavefunction satisfying the time-dependent Schrödinger equation. This wavefunction is expanded in terms of electronic molecular states j obtained by the configuration interaction method modified by inclusion of a pseudopotential for representing core electrons. Slater-type orbitals are employed as basis functions. This expansion leads to coupled first-order differential equations for the expansion coefficients $c_j(t)$. These coupled equations are solved with the initial conditions that $c_i(t = -\infty) = 1$ and that all other coefficients are zero. Let c_{if} denote the limit $c_f(t \rightarrow +\infty)$ thus calculated. Then the differential capture cross section in the centre-of-mass coordinate system is calculated using the eikonal approximation (McCarroll and Salin 1968, Kimura and Lane 1989). The cross section is expressed for a small scattering angle as:

$$\frac{d\sigma_{if}}{d\Omega} = \left| \mu v_P \int_0^\infty b \, db c_{if} \, J_{|m|}(\mu v_P b \sin\theta) \right|^2 \tag{7}$$

for $i \neq f$, where μ is the reduced mass between the projectile and the target, b the impact parameter, $J_{|m|}$ a Bessel function of order $|m|$ where m is the difference between the initial

and final projections of the electronic angular momentum onto the molecular axis, θ the scattering angle, and Ω the solid angle of the scattered projectile. The integral cross section is calculated to be

$$\sigma_{if} = 2\pi \int_0^\infty b\,\mathrm{d}b\,|c_{if}|^2. \tag{8}$$

The differential cross section (7) may be transformed into that in the laboratory frame as a function of the recoil-ion momentum. Then we obtain

$$\frac{\mathrm{d}\sigma_{if}}{\mathrm{d}p_{\perp \mathrm{R}}} = 2\pi \frac{\tan\theta}{\mu v_{\mathrm{P}}} \frac{\mathrm{d}\sigma_{if}}{\mathrm{d}\Omega}. \tag{9}$$

In a previous study (Fritsch and Lin 1991), it was found that the two electrons in He react practically independently in this collision energy regime. Thus, for the pure electron capture process (4), the He atom was treated as a one-electron system in which the electron moves in a pseudopotential. In other words, two electrons out of three were explicitly taken into account. Test calculations revealed that the cross sections for $n \leqslant 3$ are negligibly small (lower than 5% of the total cross section), as expected from the adiabatic molecular potential-energy curves and hence those channels below $n = 4$ are ignored in the calculation. Five Σ molecular states were included in the close-coupling equations, namely the initial channel and the charge-transfer channels nl = 4s, 4p, 5s and 5p. Capture to $n = 5$ was found to be dominant, contributing about 90% of the total cross section. The predicted oscillations in $\mathrm{d}\sigma_{if}/\mathrm{d}p_{\perp \mathrm{R}}$ due to an interference between amplitudes associated with different trajectories are smeared out to some extent, as is found in figure 4, after convolution with the experimental momentum resolution of ± 0.2 au. The interference pattern observed by the theory may be washed out if a larger basis set is used in the calculation. The convoluted $\mathrm{d}\sigma/\mathrm{d}p_{\perp \mathrm{R}}$ qualitatively agrees with the present experimental cross section with a maximum at about $p_{\perp \mathrm{R}} = 1$ au, although the absolute value of the maximum differential cross section is larger than experiment by a factor of about 2.5.

5. Conclusion

From the data presented here we conclude that the new experimental method, high-resolution recoil-ion momentum spectroscopy (COLTRIMS), may provide new insight into the dynamics of capture and ionization processes, even in fast ion–atom collisions, due to its high resolution and completeness in momentum space (all recoil directions) where other methods suffer a deficiency due to the lack of sufficient resolution and efficiency. The close-coupling calculations for the single-electron capture channel, which take the dynamical features of the collision into account, yield a good agreement with the experimental data in the shape of the differential cross section as a function of the transverse recoil momentum. However, the absolute value of the calculated cross section is larger than the experimental data by a factor of 2.5 and the interference structure predicted in the calculations is not observed. The principal quantum number n of the captured electron and the critical internuclear distance R were studied in the classical overbarrier model for the capture processes (single-electron capture and transfer ionization). However, it totally fails in predicting the absolute value of the capture cross section.

Acknowledgments

Four of us (OJ, VM, BD, HS-B) want to thank the Institute of Physical and Chemical Research (RIKEN) for support. One of the authors (VM) was supported by the Deutsche

Forschungsgemeinschaft and the Studienstiftung des Deutschen Volkes. We are indebted for many helpful discussions in the development of COLTRIMS to our colleagues J Ullrich, R Dörner and L Spielberger.

References

Ali R, Frohne V, Cocke C L, Stockli M, Cheng S and Raphaelian M L A 1992 *Phys. Rev. Lett.* **69** 2491

Barat M, Gaboriaud M N, Guillemot L, Roncin P, Laurent H and Andriamonje S 1987 *J. Phys. B: At. Mol. Phys.* **20** 5771

Barat M and Roncin P 1992 *J. Phys. B: At. Mol. Opt. Phys.* **25** 2205 and other references therein

Belkić Dž and Gayet R 1977 *J. Phys. B: At. Mol. Phys.* **10** 1923

Bordenave-Montesquieu A, Benoit-Cattin P, Boudjema M, Gleizes A and Bachau H 1987 *J. Phys. B: At. Mol. Phys.* **20** L695

Brusdeylins G, Toennies J T and Vollmer R 1989 *XII Symp. on Molecular Beams, Perugia 1989* Abstracts p 98

Chetioui A *et al* 1990 *J. Phys. B: At. Mol. Opt. Phys.* **23** 3659

Cocke C L, Giese J P, Tunnell L N, Waggoner W and Varghese S L 1986 *Proc. 14th Int. Conf. on the Physics of Electronic and Atomic Collisions 1985 (Palo Alto)* ed D C Lorents, W E Meyerhof and J R Peterson (Amsterdam: North-Holland) Invited papers p 453 and references therein

Dillingham T R, Macdonald J R and Richard P 1981 *Phys. Rev.* **24** 1237

Fritsch W and Lin C D 1991 *Phys. Rep.* **202** 1

Frohne V 1993 *PhD Thesis* Kansas State University

Frohne V, Cheng S, Ali R, Raphaelian M, Cocke C L and Olson R E 1993 *Phys. Rev. Lett.* **71** 696

Giese J P, Cocke C L, Waggoner W, Tunnell L N and Varghese S L 1986 *Phys. Rev.* A **34** 3770

Giese J P, Wu W, Ben-Itzhak I, Cocke C L, Ali R, Richard P, Stöckli M and Schöne H 1993 *Proc. 18th Int. Conf. on the Physics of Electronic and Atomic Collisions 1993 (Aarhus)* (AIP Conf. Proc. **295**) ed T Andersen, B Fastrup, F Folkmann, H Knudsen and N Andersen (New York: AIP) Invited papers p 585

Htwe W T, Vajnai T, Barnhart M, Gaus A D and Schulz M 1994 *Phys. Rev. Lett.* **73** 1348

Itoh A, Schneider D, Schneider T, Zouros T J M, Nolte G, Schiwietz G, Zeitz W and Stolterfoht N 1985 *Phys. Rev.* A **31** 684

Kimura M and Lane N F 1989 *Advances in Atomic, Molecular and Optical Physics* vol 26 (San Diego: Academic) p 79

Lawrence G P, Fan C Y and Bashkin S 1972 *Phys. Rev. Lett.* **28** 1612

Leventhal M, Murnick D E and Kugel H W 1972 *Phys. Rev. Lett.* **28** 1609

Lorents D C and Aberth W 1965 *Phys. Rev.* A **139** 1017 and other references therein

Mack 1987 *PhD Thesis* Rijksuniversiteit Utrecht

McCarroll R and Salin A 1968 *J. Phys. B: At. Mol. Phys.* **1** 163

Meng L, Olson R E, Dörner R, Ullrich J and Schmidt-Böcking H 1993 *J. Phys. B: At. Mol. Opt. Phys.* **26** 3387

Mergel V 1994 *Diplomthesis* University Frankfurt

Mergel V *et al* 1995 *Phys. Rev. Lett.* **74** 2200

Morgenstern R, van der Straten P and Niehaus A 1990 *Phys. Rev. Lett.* **64** 2589

Nielsen E H, Andersen L H, Bárány A, Cederquist H, Heinemeier J, Hvelplund P, Knudsen H, MacAdam K B and Sørensen J 1985 *J. Phys. B: At. Mol. Phys.* **18** 1789

Ohtani S 1984 *Proc. 13th Int. Conf. on Physics of Electronic and Atomic Collisions 1983 (Berlin)* ed J Eichler, I V Hertel and N Stolterfoht (Amsterdam: North-Holland) Invited papers p 353

Ohtani S, Kaneko Y, Kimura M, Kobayashi N, Iwai T, Matsumoto A, Okuno K, Takagi S, Tawara H and Tsurubuchi S 1982 *J. Phys. B: At. Mol. Phys.* **15** L533

Park J T, Aldag J E, Peacher J L and George J M 1978 *Phys. Rev. Lett.* **40** 1646

Ryufuku H, Sasaki K and Watanabe T 1980 *Phys. Rev.* A **21** 745

Schmeissner C, Cocke C L, Mann R and Meyerhof W 1984 *Phys. Rev.* A **30** 1661

Schuch R, Schöne H, Miller P D, Krause H F, Dittner P F, Datz S and Olson R E 1988 *Phys. Rev. Lett.* **60** 925

Shinpaugh J L, Sanders J M, Hall J M, Lee D H, Schmidt-Böcking H, Tipping T N, Zouros T J M and Richard P 1992 *Phys. Rev.* A **45** 2922

Tawara H, Iwai T, Kaneko Y, Kimura M, Kobayashi N, Matsumoto A, Ohtani S, Okuno K, Takagi S and Tsurubuchi S 1984 *Phys. Rev.* A **29** 1529

Tsurubuchi S, Iwai T, Kaneko Y, Kimura M, Kobayashi N, Matsumoto A, Ohtani S, Okuno K, Takagi S and Tawara H 1982 *J. Phys. B: At. Mol. Phys.* **15** L733

Ullrich J, Dörner R, Mergel V, Jagutzki O, Spielberger L and Schmidt-Böcking H 1994 *Comment. At. Mol. Phys.* **30** 285

Wu W *et al* 1994 *Phys. Rev. Lett.* **72** 3170

Wu W, Wong K L, Cocke C L, Giese J P and Montenegro E C 1995 *Phys. Rev.* A **51** 3718